Sonolytic Decomposition of Ozone in Aqueous Solution: Mass Transfer Effects

ARTICLE *in* ENVIRONMENTAL SCIENCE AND TECHNOLOGY · OCTOBER 1998

Impact Factor: 5.33 · DOI: 10.1021/es980620o

2 AUTHORS:

Linda K Weavers
The Ohio State University
68 PUBLICATIONS **1,519** CITATIONS
SEE PROFILE

Michael R. Hoffmann
California Institute of Technology
378 PUBLICATIONS **30,110** CITATIONS
SEE PROFILE

Environ. Sci. Technol. **1998**, *32,* 3941−3947

Sonolytic Decomposition of Ozone in Aqueous Solution: Mass Transfer Effects

LINDA K. WEAVERS† AND MICHAEL R. HOFFMANN*

W. M. Keck Laboratories, California Institute of Technology, Pasadena, California 91125

The sonolytic degradation of ozone (O_3) was investigated in both closed and open continuous-flow systems to examine effects of mass transfer on chemical reactivity in the presence of ultrasound. Degradation of O_3 followed apparent first-order kinetics at frequencies of both 20 and 500 kHz in all the systems. Degassing of O_3 was observed at 20 kHz due to the effects of rectified diffusion and larger resonant radii of the cavitation bubbles than at 500 kHz. Increased mass transfer of O_3 diffusing into solution due to ultrasound as measured by the mass transfer coefficient, k_La_2, was observed at both frequencies. At 20 kHz, an increase in mass transfer rates in the presence of ultrasound may be partially attributed to turbulence induced by acoustic streaming. However, the main process of increased gas−liquid mass transfer in the presence of ultrasonic waves appears to be due to the sonolytic degradation of O_3 creating a larger driving force for gaseous O_3 to dissolve into solution. From first-order cyclohexene degradation kinetics obtained by sonolysis, ozonolysis, sonolytic ozonolysis, and comparing the large diameter of an O_3 diffusing gas bubble to the size of an active cavitation bubble, it appears that diffusing gas bubbles containing O_3 are not directly influenced by ultrasonic fields.

Introduction

A number of advanced oxidation processes (AOPs) using ozone have been developed to destroy a variety of chemical contaminants in water. These processes including ozonation at high pH, ozonation combined with hydrogen peroxide, and ozonation combined with ultraviolet irradiation are based on the in situ decomposition of ozone to form hydroxyl radical leading to the initiation of a free-radical chain reaction (*1*−*4*).

Ozonation combined with ultrasonic irradiation (sonolysis) is a similar, although less developed AOP. Ultrasonic irradiation has been investigated for the destruction of aqueous organic and inorganic pollutants (*5*−*12*). Sound waves just above the audible range produce cavitation bubbles. Upon collapse of these bubbles, high temperatures and pressures are generated inside the bubble. The chemical destruction of compounds has been demonstrated to occur inside either imploding bubbles, or in the supercritical interfacial sheaths surrounding the bubbles either by direct pyrolysis or by hydroxylation resulting from the gas-phase pyrolysis of H_2O. The addition of ozone into sonolytic systems has been demonstrated to increase the net transformation rates of a wide range of chemical species (*13*−*21*).

The thermal decomposition of ozone in collapsing cavitation bubbles appears to be the main mechanism for the enhanced destruction of chemical contaminants (*13*). Ozone decomposes into oxygen and atomic oxygen as follows:

$$O_3 \xrightarrow{M} O2 + O(^3P) \quad (1)$$

atomic oxygen then reacts with H_2O vapor to form hydroxyl radical: (*22*, *23*)

$$O(^3P) + H_2O \rightarrow 2OH^{\bullet} \quad (2)$$

In addition, previous studies have reported increased mass transfer coefficients, k_La, of ozone diffusing into solution in the presence of ultrasound (*16*, *19*, *21*). k_L is the mass transfer velocity (cm/s) and a is the specific interfacial area for mass transfer (cm^2/cm^3). Olson and Barbier (*21*) hypothesized that the apparent enhancement was due to mechanical effects such as greater mixing and break up of gas bubbles as they enter an ultrasonic reactor.

Ultrasonic degassing has many commercial applications. For example, the ultrasonic treatment of liquids is currently used in industry to degas carbonated drinks, photographic solutions, and other liquids such as molten metals, electroplating solutions, and beer. Equipment in the 20 to 40 kHz range is typically used (*24*−*27*). Degassing may be a factor in sonolytic ozonation due to the high Henry's Law constant of ozone ($H = 1.08 \times 10^4$ Pa·m^3/mol) (*28*), especially at low frequency.

The primary objective of this study was to explore the various mass transfer mechanisms occurring during sonolytic ozonation. By investigating the decomposition of ozone in a continuously stirred tank reactor (CSTR) mode under conditions closed to the atmosphere, open to the atmosphere, and open to the atmosphere with ozone gas bubbling, mass transfer coefficients were determined. The role of degassing in the sonolytic ozonation system was also investigated. Cyclohexene degradation experiments were used to determine the interactions of a diffusing ozone bubble with an ultrasonic field. Two ultrasonic frequencies, 20 and 500 kHz, were employed for all experiments.

Experimental Methods

Materials and Reagents. Cyclohexene (Aldrich, 99+%) and perchloric acid (Mallinckrodt, 70%) were used as received. All solutions were prepared with water purified by a Millipore Milli-Q UV Plus system (R = 18.2 MΩ cm).

Ozone Experiments. The experimental setup, shown in Figure 1, consisted of a 2-L water-jacketed glass reactor to continually saturate solutions with ozone, a water-jacketed glass reactor for sonication reactions capable of operating either open or closed to the atmosphere, a source of ultrasound, a Masterflex peristaltic pump (Cole-Parmer) to pump aqueous solutions between the reactors, and a diode array spectrophotometer (Hewlett-Packard, model 8452A). The temperature of the bulk, aqueous ozone solution was maintained constant at 23 ± 3 °C (Haake, Model A81 Temperature Regulator set at 20 ± 0.1 °C) by using water jackets on both reactors. Tubing in contact with gaseous or aqueous ozone was Teflon except at connections and in the pump where Viton was used.

* Corresponding author telephone: (626) 395-4391; Fax: (626) 395-3170; e-mail: mrh@cco.caltech.edu.

† Present address: Department of Civil and Environmental Engineering and Geodetic Science, The Ohio State University, Columbus, OH 43210. E-mail: weavers.1@osu.edu.

10.1021/es980620o CCC: $15.00
Published on Web 10/29/1998

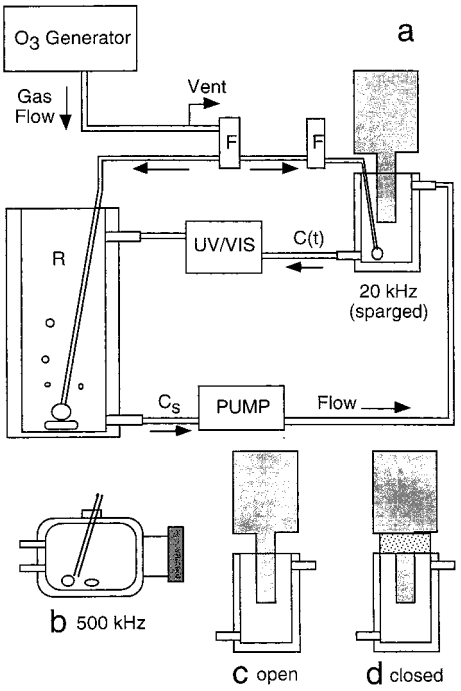

FIGURE 1. (a) Schematic diagram of the reactor system configured for 20 kHz system open to the atmosphere with gas bubbling; (b) 500 kHz ultrasonic reactor shown configured open to the atmosphere with gas bubbling; (c) 20 kHz reactor configured open to the atmosphere; and (d) 20 kHz reactor in closed system configuration. Abbreviations: 20 kHz, 20 kHz ultrasonic probe reactor ($V = 235$ mL); 500 kHz, 515 kHz ultrasonic reactor ($V = 475$ mL); F, gas flowmeter; R, O_3 saturated reservoir.

Oxygen gas was filtered through Drierite and a molecular sieve (Alltech), and through an activated-charcoal hydrocarbon trap (Alltech) before introduction to an OREC ozonator (Model O3V10-O) at 0.6 atm and 4.5 L min^{-1}. The O_2/O_3 gas mixture entered the reactors at a flowrate of 4 L min^{-1}. During open system operation with gas bubbling, 100 mL min^{-1} flowed out of a fritted-glass gas diffuser into the sonication reactor. In open and closed experiments, the 100 mL min^{-1} flow was vented during sonication. The O_3 gas-phase concentrations were determined by oxidation of indigo trisulfonic acid as described by Bader and Hoigné (*29*).

The sonications at 500 kHz were performed with an ultrasonic transducer (Undatim Ultrasonics) operating at 515 kHz with a reaction volume of 475 mL. The 20 kHz reactor was a direct immersion probe system (VCX-400 Vibracell, Sonic & Materials) with a volume of 235 mL. The total volume of the circulating solution was 2 L for the 500 kHz reactor and 1.5 L for the 20 kHz probe. The emitting areas of the transducers were 25.5 and 1.20 cm^2 for the 500 and 20 kHz systems, respectively. The ultrasonic power inputs into the aqueous solution were measured by calorimetry (*25*). The 20 kHz probe was tuned in air, and the titanium tip was polished prior to each sonication. Turbulence from the oxygen sparging was assumed to be sufficient for complete mixing in the 20 kHz reactor while a magnetic stirrer was used in the 500 kHz reactor.

Ozone decomposition is accelerated at high pH (*30*). To minimize the chain decomposition reactions of ozone with OH^-, all experiments were run at pH 2. Ultrapure water was adjusted to pH 2 with concentrated $HClO_4$ at a net ionic strength of 0.01 M. Measurements made before and after the experiments did not show a significant change in the pH. The aqueous solution was continually pumped at 95 mL min^{-1} from the saturated ozone reservoir to the ultrasonic reactor, through the spectrophotometer, and back to the saturated ozone reservoir. Since the flowrate was much smaller than the volume of the reservoir, the reservoir was assumed to maintain a constant aqueous ozone concentration throughout the experiment. Aqueous ozone concentrations were measured spectrophotometrically at $\lambda = 260$ nm ($\epsilon = 3292\ M^{-1}\ cm^{-1}$) (*31*). Particles and bubbles generated from sonication were not observed to interfere with absorbance measurements. During initiation of an experiment, ozone was bubbled into both reactors with the solution circulating. Once a steady-state ozone saturation was obtained, ultrasound was applied until a second steady-state ozone concentration was achieved.

Saturated aqueous-phase concentrations of ozone were determined and achieved for all ozone gas concentrations used. All ozone decomposition experiments were performed in triplicate. Error bars on graphs represent experiment to experiment variation.

Cyclohexene Oxidation. The sonolytic oxidation of cyclohexene was studied under batch reactor conditions in both ultrasonic reactors. Initial solutions containing 2.5 mM of cyclohexene were adjusted to pH 2 with $HClO_4$. Measurements made before and after the experiments did not show a significant change in pH. To initiate a kinetic run, oxygen bubbling, ultrasound, and/or voltage from the ozonator was applied. In the 20 kHz reactor, 20 mL min^{-1} of gas were bubbled through the solution while 40 mL min^{-1} of gas were bubbled through solution in the 500 kHz reactor.

Sample aliquots of 2.0 mL were collected at designated times and transferred to vials without a free headspace. Due to the rapid reaction rate of ozone with cyclohexene, residual ozone was below detection. All samples were filtered before analysis with 0.2-μm Teflon syringe filters (Gelman). Quantification of cyclohexene was achieved with a Hewlett-Packard gas chromatograph (HP 5890 series II, GC) with a mass-selective detector (HP 5989A-MSD). A 0.32 mm × 25 m FFAP chromatographic column (Hewlett-Packard) was used for GC separation.

Results

To observe the effects of mass transfer enhancement and degassing of ozone due to sonication, experiments were performed with the ultrasonic reactor closed to the atmosphere (closed), open to the atmosphere (open) to observe degassing, and open to the atmosphere with gas bubbling (sparged) to observe enhanced mass transfer of ozone to solution. The three different systems will be referred to as closed, open, and sparged, respectively. The sonication reactor system was treated as a continuously stirred tank reactor (CSTR). By solving the corresponding mass balance equations for the three different systems, reaction rate constants and mass transfer coefficients were determined for each scenario. The general mass balance equation for the CSTR reactor is given as

$$\frac{dM}{dt} = \frac{dC(t)}{dt}V = qC_s - qC(t) - rV \qquad (3)$$

where $C(t)$ is the ozone concentration (μM) in the ultrasonic reactor, V is the sonicated volume (L) in the ultrasonic reactor, C_s is the ozone concentration (μM) in the saturated ozone reservoir, q is the volumetric flowrate (L min^{-1}) of aqueous ozone between reactors, and r is the combined first-order reaction rate (μM min^{-1}) for all ozone loss mechanisms due to ultrasound. In the case of the closed system, the mass balance equation becomes:

$$\frac{dC(t)}{dt} = \frac{q}{V}[C_s - C(t)] - kC(t) \qquad (4)$$

where k is the first-order reaction rate coefficient (min^{-1}) for the degradation of ozone by sonication and assuming that the volume occupied by bubbles in the sonicating reactor is negligible. The open system has additional loss terms due to the sonolytically induced degassing of ozone shown by

$$\frac{dC(t)}{dt} = \frac{q}{V}[C_s - C(t)] - kC(t) - k_L a'\left[C(t) - \frac{C_g(t)}{H}\right] - k_L a''\left[C(t) - \frac{C_g''(t)}{H}\right] \quad (5)$$

where a′ and a″ are the specific interfacial areas for the top of the reactor and sonication bubbles, respectively; $C_g'(t)$ and $C_g''(t)$ are the gaseous O_3 concentrations at the top of the reactor and in the degassing bubbles, respectively; and H is Henry's Law constant. Assuming that $C_g'(t)$ and $C_g''(t)$ are negligible and combining a' and a'' ($a_1 = a' + a''$) the equation collapses to

$$\frac{dC(t)}{dt} = \frac{q}{V}[C_s - C(t)] - [k + k_L a_1]C(t) \quad (6)$$

The sparged system has another mass-transfer term resulting from ozone diffusing from a gas bubble in the presence of ultrasound, $k_L a_2$ (min^{-1}). The sparged system is represented as

$$\frac{dC(t)}{dt} = \frac{q}{V}[C_s - C(t)] - [k + k_L a_1]C(t) + k_L a_2[C_s - C(t)] \quad (7)$$

Equation 7 is valid if the volume of gas in the reactor is negligible and the ozone concentration in the diffusing gas bubble does not change significantly as it passes through the sonicating reactor. In our experiments, given that the rate of rise of a 1-mm bubble in water is 30 cm s^{-1} (*32*), the liquid height in the reactor is 20 cm, and the gas flowrate in the ultrasonic reactor is 1.67 mL s^{-1}; a diffusing gas bubble exits the reactor in <1 s. Thus, the volume of gas in the reactor is less than 2 mL (<1% of the ultrasonic volume) and the O_3 gas concentration in the diffusing gas bubble was expected to remain approximately constant. Combining terms in the three cases we obtain a generalized equation of the following form:

$$\frac{dC(t)}{dt} = AC(t) + BC_s \quad (8)$$

where in the closed, open, and sparged systems, respectively, A and B are

$$A = k + \frac{q}{V} \qquad B = \frac{q}{V} \qquad \text{(closed)} \quad (9)$$

$$A = k + \frac{q}{V} + k_L a_1 \qquad B = \frac{q}{V} \qquad \text{(open)} \quad (10)$$

$$A = k + \frac{q}{V} + k_L a_1 + k_L a_2 \qquad B = \frac{q}{V} + k_L a_2 \qquad \text{(sparged)} \quad (11)$$

Integrating with initial conditions: $t = 0, C = C_s$, and applying the boundary conditions $t = \infty$, $C = C_\infty$, we obtain

$$C(t) - C_\infty = (C_s - C_\infty)\, e^{-At} \quad (12)$$

where

$$C_\infty = \frac{BC_s}{A} \quad (13)$$

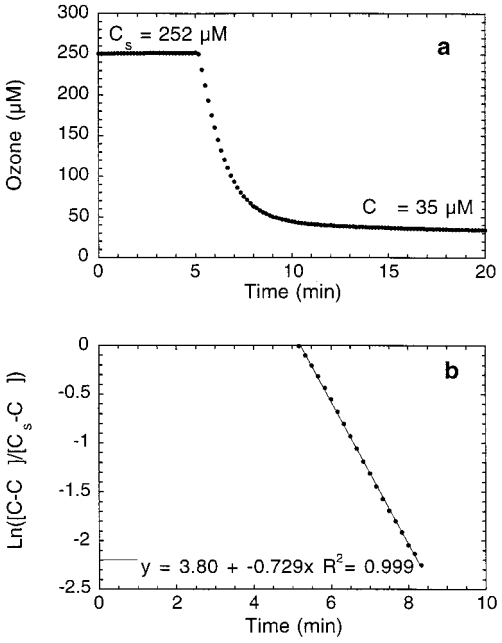

FIGURE 2. (a) Ozone decomposition in the 500 kHz sonication reactor in closed system configuration and (b) first-order degradation of O_3 in 500 kHz reactor. Power density = 96 W L^{-1}; C_s = 245 µM; pH = 2.

TABLE 1. First-Order Reaction Rate Constants for the Sonochemical Degradation of Ozone at 20 and 500 kHz

initial aqueous concentrated (µM)	k_{20} (min^{-1})	k_{500} (min^{-1})
85 ± 5	-	0.62 ± 0.09
140 ± 4	0.67 ± 0.10	0.62 ± 0.17
200 ± 4	0.77 ± 0.04	0.69 ± 0.18
245 ± 3	0.84 ± 0.07	0.66 ± 0.08

k, $k_L a_1$, and $k_L a_2$ are obtained as follows:

$$k = (A - B)_{closed} \quad (14)$$

$$k_L a_{1\ open} = (A - B)_{open} - (A - B)_{closed} \quad (15)$$

$$k_L a_{1\ sparged} = (A - B)_{sparged} - (A - B)_{closed} \quad (16)$$

$$k_L a_2 = B_{sparged} - B_{open} \quad (17)$$

Figure 2 shows results from the decomposition of ozone with the 500 kHz sonication reactor in the closed system configuration at a power density of 96 W L^{-1} and 2% w/w ozone in the gas phase. The first-order plot in Figure 2b demonstrates the first-order kinetics over four half-lives. Open and sparged system experiments at 500 kHz as well as experiments at 20 kHz were also found to be first-order. Four different aqueous ozone concentrations corresponding to ozone gas concentrations were used. As shown in Table 1, first-order degradation rate constants in the 500 kHz reactor at a power density of 96 W L^{-1} demonstrate first-order kinetics both as a function of time and concentration. In the 20 kHz reactor, at a power density of 263 W L^{-1}, the first-order degradation rate constant increased slightly as a function of increasing concentration. This is opposite to the trend observed by De Visscher et al. (*12*) for the degradation of volatile organic compounds and not nearly as significant. They observed a 3-fold increase in k with decreasing the initial concentration by a factor of 3. Our 20 kHz results show a 25% increase in k upon increasing the initial concentration by a factor of 1.75. The specific heat (C_p) of

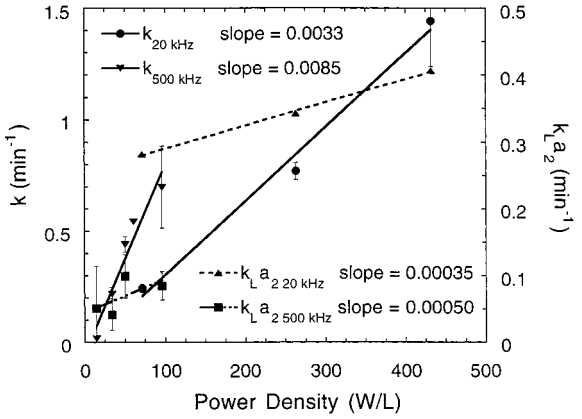

FIGURE 3. First-order degradation rate coefficient, *k*, and mass transfer coefficient, k_La_2, due to sonication vs power density at 20 and 500 kHz. Gas flowrate = 100 mL min^{-1}; pH = 2; 1.3% w/w O_3 in O_2 gas.

O_3 is 39 J mol^{-1} K^{-1} (*33*) which is similar to oxygen (30 J mol^{-1} K^{-1}) and water vapor (36 J mol^{-1} K^{-1}) (*34*). In comparison, many organic compounds have considerably higher specific heats (~120 J mol^{-1} K^{-1}), lowering the temperature in the bubble, and thus decreasing the reaction rate constants at high concentrations. Also, thermolytic destruction of O_3 is exothermic, raising the temperature in the bubble. Therefore, our results are consistent with the theory of De Visscher et al. (*12*) which suggests that C_p influences the maximum temperature achieved in a collapsing cavitation bubble.

The effect of ultrasonic power was investigated at 20 and 500 kHz with 1.3% w/w O_3 in the gas stream. Figure 3 shows a linear dependence of the first-order degradation rate constant on power density (power input/volume sonicated) at both frequencies. The slope of *k* was 2.6 times steeper in the 500 kHz reactor than with the 20 kHz probe. In both systems with no power applied, the degradation of O_3 was negligible. The rate equation for the degradation of O_3 by sonolysis at constant pH, *T*, and μ is

$$-\frac{d[O_3]}{dt}[O_3]\,\gamma P \qquad (18)$$

where $[O_3]$ is the O_3 concentration in solution, γ is the slope of the curves in Figure 3 (3.3×10^{-3} and 8.5×10^{-3} L min^{-1} W^{-1} at 20 and 500 kHz, respectively), and *P* is the power density. Therefore, with the same amount of power input per volume sonicated, O_3 was destroyed energetically more efficiently at 500 kHz. In contrast, Barbier and Pétrier observed a more rapid sonochemical degradation of O_3 at 20 kHz (*17*). At an equivalent power density, we observed a considerably larger first-order degradation rate constant at 500 kHz (0.85 min^{-1} for this study compared to 0.17 min^{-1}) but at 20 kHz the first-order degradation rate constant was similar to that reported by Barbier and Pétrier (0.33 min^{-1} for this study compared to 0.29 min^{-1}). A variety of reasons could account for the differences between the studies including the reactor geometries, the volume of solution sonicated, the area of radiating surface, and the experimental setup (CSTR without headspace vs batch with recirculating headspace).

The mass transfer coefficient of ozone entering solution by bubbling during sonication, k_La_2, also followed a linear trend as seen in Figure 3. k_La_2 increased more rapidly by a factor of 1.5 with power density at 500 kHz than at 20 kHz. However, by extrapolating to 0 power density, k_La_2 was still significant at both frequencies. The 20 kHz probe had k_La_2 values approximately 4 times greater than the 500 kHz reactor over the power density range studied.

TABLE 2. Mass Transfer Coefficients of Ozone Loss Due to Degassing in the Presence of Ultrasound with $C_s = 200\ \mu$M

		k_La_1 (min^{-1})	
ultrasonic frequency (kHz)	power density (W L^{-1})	open	sparged
20	71.1	0.12 ± 0.02	0.03 ± 0.04
20	263.0	0.42 ± 0.05	0.16 ± 0.25
20	431.9	0.17 ± 0.22	0.08 ± 0.24
500	14.5	0.005 ± 0.004	−0.004 ± 0.004
500	33.7	−0.029 ± 0.046	−0.063 ± 0.050
500	50.3	0.011 ± 0.044	0.003 ± 0.054
500	96.0	0.04 ± 0.21	−0.084 ± 0.22

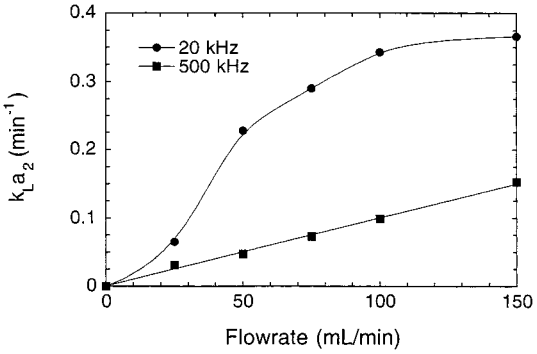

FIGURE 4. Mass transfer coefficient, k_La_2, vs gas flowrate at 20 and 500 kHz. 1.3% w/w O_3 in O_2 gas; pH = 2; power density = 50.3 W L^{-1} at 500 kHz and 263 W L^{-1} at 20 kHz.

In Table 2 the dependence of the ozone mass transfer coefficient for degassing during sonication, k_La_1, on power density is shown. The results are shown for k_La_1 in the open system and in the sparged system. The open system experiments show evidence of degassing with the 20 kHz probe. The mass transfer coefficient appeared to be largest at a moderate power and approximately a factor of 3 smaller at both lower and higher power densities. However, k_La_1 was considerably smaller in the sparged system and within experimental error of $k_La_1 = 0$ min^{-1}, indicating that degassing was not occurring when O_3 was bubbled during sonolysis. In the 500 kHz reactor degassing was not observed. All of the values were within the error limits of $k_La_1 = 0$ min^{-1} for these experiments.

The effect of increasing the O_2/O_3 gas flowrate in the ultrasonic reactor from 0 to 150 mL min^{-1} was observed in the 20 and 500 kHz system. Increasing the flowrate corresponded to a larger net surface area for mass transfer of O_3 to solution. As shown in Figure 4, k_La_2 increased linearly with flowrate in the 500 kHz reactor. With the 20 kHz probe, k_La_2 rose rapidly and reached an apparent saturation value. The increase in k_La_2 was a stronger function of flowrate in the 20 kHz system than in the 500 kHz reactor; however, the power input was not the same in these reactors.

In addition, the variation of the mass transfer coefficient due to sonication, k_La_2, was examined with different sized glass-frit diffusers ranging from a glass tube to a coarse fritted diffuser. The pore size diameters of the coarse and extra coarse frit were 40−60 μm and 170−220 μm, respectively, while the diameter of the opening on the tube without a diffuser frit was approximately 1 mm. Changing the frit size but using the same flowrate of gaseous O_3, altered the effective bubble size and the interfacial surface area for ozone diffusing into solution. The largest frit size corresponded to the smallest surface area (i.e., no frit) and the smallest frit size, coarse, yielded the largest interfacial surface area. Figure 5 illustrates that the decrease in frit size corresponded to an increase in k_La_2 in the 500 kHz reactor. As observed with the

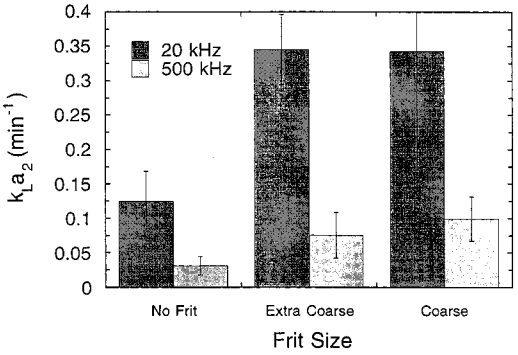

FIGURE 5. Mass transfer coefficient, $k_L a_2$, vs diffuser frit size at 20 and 500 kHz. 1.3% w/w O_3 in O_2 gas; pH = 2; power density = 50.3 W L^{-1} at 500 kHz and 263 W L^{-1} at 20 kHz. Pore diameters of frits: extra coarse = 170−220 μm; coarse = 40−60 μm; no frit = 1−1.5 mm opening.

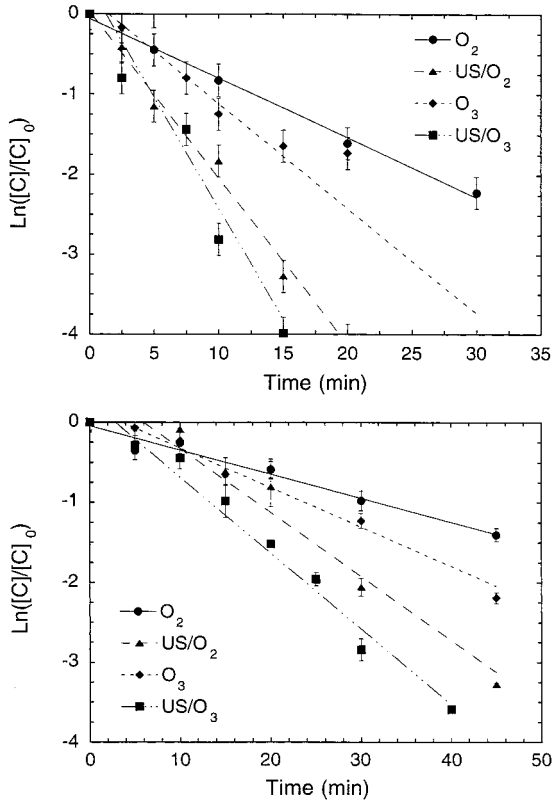

FIGURE 6. First-order degradation of cyclohexene due to oxygen bubbling, sonication with oxygen, ozonation, and sonolytic ozonation in the 20 kHz (top) and 500 kHz (bottom) reactors. O_3 gas flowrate = 20 mL min^{-1}; O_3 gas concentration = 0.66% w/w O_3 in O_2 gas; pH = 2; initial concentration of substrate = 2.5 mM; power density = 263 W L^{-1}.

increase of the O_3 gas flowrate, in the 20 kHz system, $k_L a_2$ initially increased then reached an apparent saturation value.

Loss of 2.5 mM cyclohexene by oxygen bubbling, sonication with O_2, ozonation, and sonolytic ozonation was observed in the 20 and 500 kHz reactors configured as batch reactors. Figure 6 shows the results of batch degradation experiments with the 20 kHz probe and 500 kHz reactor. Loss by these processes followed-pseudo first-order kinetics as shown by the linearity of the curves in Figure 6. The Henry's Law constant, H, is large for cyclohexene (H = 4568 Pa m^3 mol^{-1}) (*35*); therefore, loss by O_2 bubbling was due to volatilization not oxidation. The gas flowrate per volume of solution was the same in both reactors yet volatilization was larger in the 20 kHz reactor ($k_{O_2,20}$ = 0.074 min^{-1}, $k_{O_2,500}$ = 0.030 min^{-1}). Different geometries of the reactors account for the larger volatilization rates observed with the 20 kHz probe. The 20 kHz reactor was taller and had a larger opening to the atmosphere allowing longer contact times of the diffusing bubbles with the solution and more surface area exposed to the atmosphere than with the 500 kHz system. Since gas bubbling occurred in all experiments, the rate constant for loss due to volatilization (k_{O_2}) was subtracted from other rate constants. In Table 3 the corrected k values for each process at both frequencies are listed. In each system, degradation by sonication combined with ozonation was fastest followed by separate experiments of sonication and ozonation.

TABLE 3. Corrected First-Order Degradation Rate Constants for the Loss of Cyclohexene under Various Conditions

experiment	k_{20} (min^{-1})	k_{500} (min^{-1})
sonication w/O_2	0.134	0.050
ozonation	0.057	0.019
sonication w/O_3	0.204	0.065

Discussion

As shown in Table 2, degassing was observed only in the 20 kHz reactor. However, the highest rate of degassing occurred with a moderate power setting. Also, when adding ozone into the sonication reactor in the presence of ultrasound, the degassing effect was minimized considerably.

One possible mechanism for degassing involves rectified diffusion and bubble coalescence (*26*). First, during one bubble cycle, gas flux into the bubble during the rarefaction cycle (i.e., expansion phase of the longitudinal wave) exceeds flux out in the compression cycle. This process of rectified diffusion causes a bubble to grow more during rarefaction cycles than shrink during compression cycles. As a result of rectified diffusion, bubbles typically grow from a bubble nucleus above the Blake threshold (e.g., radius = 10^{-9} to 10^{-6} m) to a value near their resonant radius (e.g., radius = 163 μm at 20 kHz) where they cavitate. Additionally, bubbles smaller than resonant size cluster at pressure antinodes as a result of Bjerknes forces. Bubbles clustered at either pressure nodes or antinodes coalesce, and if they are large enough they will be removed by buoyancy forces (*26*). The resonant radius of a bubble in O_2 saturated water at 20 kHz is 163 μm whereas at 515 kHz it is 6.5 μm (*26*). Therefore, at 20 kHz due to the larger resonant radius, bubbles are larger when they cluster at the antinodes and coalesce. This results in a larger amount of degassing at the lower frequency. Degassing also depends on the acoustic amplitude and size of the bubble before it undergoes rectified diffusion. These dependencies may result in the maximal $k_L a_1$ at a moderate power. Lower degassing coefficients observed in the system with gas sparging may actually be due to a lower degradation rate constant, k, resulting from diffusing bubbles cushioning cavitation rather than a smaller $k_L a_1$, however we could not confirm this effect from our results.

Using different flowrates of O_2/O_3 gas and different gas diffuser-frits in the sonication reactor gave insight into the mechanical mixing effects of ultrasound at both frequencies. If mechanical effects were not important we would expect to see a linear increase in the flowrate due to a linear increase in the gas−liquid surface area for O_3 dissolving into solution. This was observed at 500 kHz; however, at 20 kHz $k_L a_2$ increased rapidly until it reached an apparent maximum at higher flowrates. Decreasing the frit size of the diffuser showed similar results. In the absence of mechanical mixing effects, an open tube diffuser yields the smallest gas−liquid interfacial surface area, whereas a coarse frit results in the greatest interfacial surface area for the same gas flowrate. At

500 kHz there was an increase in k_La_2 with increasing gas−liquid surface area but at 20 kHz an extra coarse frit had a similar k_La_2 to the coarse frit. In these experiments, the 20 kHz probe was operating at 62 W, with a radiating area of 1.2 cm^2 (P/radiating area = 52 W cm^{-2}). However, the 500 kHz transducer has a radiating area of 25.5 cm^2 and was operating at a power of 24 W (P/radiating area = 0.94 W cm^{-2}).

The nonlinear effect observed was due to greater acoustic streaming present in the 20 kHz reactor resulting in more turbulence than in the 500 kHz reactor. Acoustic streaming is caused by an energy gradient in the direction of propagation of the acoustic wave. The energy gradient corresponds to a force which when acting on a liquid causes the liquid to accelerate. The larger acoustic intensity (power input/surface area of emitter) at 20 kHz caused a larger force and hence a larger acceleration of the liquid. This resulted in more turbulence at 20 kHz. Therefore, as observed at 20 kHz, different gas−liquid interfacial surface areas yield similar amounts of mass transfer if there is considerable acoustic streaming. Since this is a mechanical effect, it is dependent on the reactor configuration. Turbulence would be reduced in a larger reactor with the same probe.

As shown in Figure 3, k_La_2 was linear with increasing power density. However, extrapolating to 0 W L^{-1} power, k_La_2 was nonzero with both the 20 and 500 kHz frequencies. Enhanced mass transfer, k_La_2, was present in both systems although there was no evidence of mechanical effects at 500 kHz. As a result of these artifacts, it seems that k_La_2 was due to sonolytic degradation of ozone. Sonochemical degradation of O_3 reduced the aqueous O_3 concentration below the saturation value in the ultrasonic reactor allowing more O_3 to diffuse into solution. Figure 3 shows that O_3 degraded faster with increasing power at both frequencies. However, the dependency on power was stronger for k than for k_La_2 as expected if sonolytic degradation of O_3 was causing enhanced mass transfer. This is due to faster degradation of aqueous O_3 by sonication than resaturation by diffusing gas bubbles. The discrepancy between the k and k_La_2 was larger at 500 kHz than at 20 kHz, which again shows the larger effect of acoustic streaming at 20 kHz.

Cyclohexene degradation by sonication, ozonation, and sonolytic ozonation was performed to investigate the effect ultrasound had on an O_3 gas bubble diffusing into solution. Cyclohexene reacts very rapidly with both O_3 ($k = 3.9 \times 10^6$ M^{-1} s^{-1}) (*36*) and $OH^\bullet$ ($k = 8.8 \times 10^9$ M^{-1} s^{-1}) (*37*). Due to its rapid reaction rate with O_3, it will react at the gas−liquid interface and no O_3 will be present in solution. Therefore, if an O_3 gas bubble is influenced by ultrasound either by the diffusing gas bubbles breaking up, by turbulence, or by O_3 being pumped into solution by the propagating ultrasound wave, a difference should be seen in the first-order degradation rate constant by sonolytic ozonation over the sum of the rate constants by sonication and ozonation. Adding the independently obtained rate constants for sonication and ozonation ($k_{US} + k_{O_3} = 0.191$ min^{-1}) at 20 kHz and comparing it to the combined process of sonolytic ozonation ($k_{US/O_3} = 0.204$ min^{-1}), the difference is only 6%. Similarly at 500 kHz, $k_{US} + k_{O_3} = 0.069$ min^{-1} and $k_{US/O_3} = 0.065$ min^{-1}; the difference is also 6%. Again, mechanical mixing effects were observed at 20 kHz by a slightly larger mass transfer rate coefficient in the combined system than the linear combination of separate experiments. However, these apparent effects were within the range of experimental error. Also, a diffusing O_3 bubble is on the order of 1000 μm in diameter but the resonant radii at which the bubble will be maximally perturbed by ultrasonic waves are 163 and 6.5 μm at 20 and 515 kHz, respectively. Hence, an O_3 bubble diffusing into solution is not influenced to a significant extent by ultrasound. O_3 first dissolves into solution and then rediffuses into a gaseous cavitation bubble where it will undergo thermolytic decomposition.

The results of these experiments have interesting implications in reactor design. In the 20 kHz reactor system, some mechanical effects of mass transfer were observed as shown in Figures 4 and 5. However, ultrasonically enhanced mass transfer is mainly a function of sonolytically degrading O_3; thus, lowering the aqueous [O_3] below saturation values which allows more O_3 to dissolve into solution as a function of time. Figure 4 demonstrates that an increased flowrate of gaseous O_3 into the sonication reactor increases ultrasonically enhanced mass transfer. An increased flowrate is expected to linearly increase mass transfer in any system simply by having more gas−liquid surface area. Cyclohexene degradation experiments revealed that the overall process of sonolytic ozonolysis involves initial dissolution of O_3 into solution; the dissolved O_3 then diffuses into a growing cavitation bubble where it is thermolytically decomposed. With the relatively low gaseous O_3 flowrates into the 20 and 500 kHz reactors for cyclohexene experiments, only slight enhanced mass transfer would be expected if O_3 was dissolving into solution rather than reacting at the gas−liquid interface. At higher O_3 flowrates, larger k_La_2 would be expected; hence, enhanced dissolution of O_3 should be observed in the combined system over the separate sonication and ozonation systems. However, the reaction rate constant of a compound with O_3 (k_{O_3}) plays an important role in the amount of enhanced degradation seen with sonolytic ozonation due to thermal decomposition of O_3 forming $OH^\bullet$ (*13*). In the design of a sonolytic ozonation process for the degradation of pollutants, the location of gaseous O_3 addition and the gas flowrate are important parameters. For example, if low gaseous O_3 flowrates are used, gaseous O_3 may be added prior to applying ultrasound to gain beneficial effects of the combined process. However, at moderate flowrates, adding gaseous O_3 in the presence of ultrasound should enhance degradation more than configuring the processes in series and applying O_3 prior to sonication. Finally, as seen in Figure 4 at 20 kHz, a maximum gaseous O_3 flowrate is desirable.

Acknowledgments

The authors thank Ralf Höchemer for valuable discussions and insight, Paul Sivilotti for help with statistical analysis, and anonymous reviewers for thoughtful comments. Financial supported provided by Defense Advanced Research Projects Agency (DARPA), the Office of Naval Research (ONR), the Electric Power Research Institute (EPRI), and the Department of Energy (DOE) is gratefully acknowledged.

Literature Cited

(1) Glaze, W. H.; Kang, J. W.; Chapin, D. H. *Ozone Sci. Eng.* **1987**, *9*, 335−352.
(2) Legrini, O.; Oliveros, E.; Braun, A. M. *Chem. Rev.* **1993**, *93*, 671−698.
(3) Masten, S. J.; Davies, S. H. R. In *Environmental Oxidants*; Nriagu, J. O., Simmons, M. S., Eds.; John Wiley & Sons: New York, 1994; pp 517−547.
(4) Peyton, G. R.; Huang, F. Y.; Burleson, J. L.; Glaze, W. H. *Environ. Sci. Technol.* **1982**, *16*, 448−453.
(5) Hua, I.; Höchemer, R. H.; Hoffmann, M. R. *Environ. Sci. Technol.* **1995**, *29*, 2790−2796.
(6) Hua, I.; Hoffmann, M. R. *Environ. Sci. Technol.* **1996**, *30*, 864−871.
(7) Kontronarou, A.; Mills, G.; Hoffmann, M. R. *J. Phys. Chem.* **1991**, *95*, 3630−3638.
(8) Kontronarou, A.; Mills, G.; Hoffmann, M. R. *Environ. Sci. Technol.* **1992**, *26*, 2420−2428.
(9) Pétrier, C.; Lamy, M.-F.; Francony, A.; Benahcene, A.; David, B. *J. Phys. Chem.* **1994**, *98*, 10514−10520.
(10) Francony, A.; Pétrier, C. *Ultrason. Sonochem.* **1996**, *3*, S77−S82.
(11) Drijvers, D.; Baets, R. D.; Visscher, A. D.; Langenhove, H. V. *Ultrason. Sonochem.* **1996**, *3*, S83−S90.

(12) De Visscher, A.; Van Eenoo, P.; Drijvers, D.; Van Langenhove, H. *J. Phys. Chem*. **1996**, *100*, 11636−11642.
(13) Weavers, L. K.; Ling, F. H.; Hoffmann, M. R. *Environ. Sci. Technol.* **1998**, 32, in press.
(14) Sierka, R. A.; Amy, G. L. *Ozone Sci. Eng.* **1985**, *7*, 47−62.
(15) Sierka, R. A. *Ozone Sci. Eng.* **1985**, *6*, 275−290.
(16) Sierka, R. A. Mass Transfer and Reaction Rate Studies of Ozonated MUST Wastewaters in the Presence of Sound Waves. University of Arizona, 1976.
(17) Barbier, P. F.; Pétrier, C. *J. Adv. Oxid. Technol.* **1996**, *1*, 154−159.
(18) Chen, J. W. *Water* **1972**, *69*, 61−70.
(19) Dahi, E. *Water Res.* **1976**, *10*, 677−684.
(20) Höchemer, R. H. Ph.D. Thesis, California Institute of Technology, 1996.
(21) Olson, T. M.; Barbier, P. F. *Water Res.* **1994**, *28*, 1383−1391.
(22) Hart, E. J.; Henglein, A. *J. Phys. Chem*. **1986**, *90*, 3061−3061.
(23) Hart, E. J.; Henglein, A. *J. Phys. Chem*. **1985**, *89*, 4342−4347.
(24) Brown, B.; Goodman, J. E. *High-Intensity Ultrasonics*; D. Van Nostrand: Princeton, 1965.
(25) Mason, T. J.; Lorimer, J. P. *Sonochemistry: Theory, Applications and Uses of Ultrasound in Chemistry*; Ellis Horwood Ltd: Chichester, 1988.
(26) Leighton, T. G. *The Acoustic Bubble*; Academic Press: London, 1994.
(27) Suslick, K. S. *Ultrasound: Its Chemical, Physical, and Biological Effects*; VCH Publishers: New York, 1988.
(28) Seinfeld, J. H. *Atmospheric Chemistry and Physics of Air Pollution*; Wiley-Interscience: New York, 1986.
(29) Bader, H.; Hoigné, J. *Water Res.* **1981**, *15*, 449−456.
(30) Sehested, K.; Corfitzen, H.; Holcman, J.; Fischer, C. H.; Hart, E. J. *Environ. Sci. Technol.* **1991**, *25*, 1589−1596.
(31) Hart, E. J.; Sehested, K.; Holcman, J. *Anal. Chem*. **1983**, *55*, 46−49.
(32) Haberman, W. L.; Morton, R. K. *Trans. Am. Soc. Civ. Eng.* **1956**, *121*, 233.
(33) Chase, M. W., Jr.; Davies, C. A.; Downey, J. R. J.; Frurip, D. J.; McDonald, R. A.; Syverud, A. N. *J. Phys. Chem. Ref. Data, Suppl. 1*, **1985**, *14*, 1−1856.
(34) Perry, R. H.; Green, D. *Perry's Chemical Engineers' Handbook*; McGraw-Hill: New York, 1984.
(35) Mackay, D.; Shiu, W. Y.; Ma, K. C. Volatile Organic Chemicals. *Illustrated Handbood of Physical-Chemical Properties and Environmental Fate for Organic Chemicals*; Lewis Publishers: Boca Raton, 1991; Vol. III.
(36) Kuo, C. H. Reactions of Dissolved Pollutants with Ozone in Aqueous Solutions. Mississippi State University, 1984.
(37) Buxton, G. V.; Greenstock, C. L.; Helman, W. P.; Ross, A. B. *J. Phys. Chem. Ref. Data* **1988**, *17*, 513−817.

Received for review June 16, 1998. Revised manuscript received September 21, 1998. Accepted September 29, 1998.

ES980620O